

AI based on frequency slicing deep neural network for underwater visible light communication

Nan CHI*, Fangchen HU, Guoqiang LI, Chaofan WANG & Wenqing NIU

Key Laboratory for Information Science of Electromagnetic Waves (MoE), Fudan University, Shanghai 200433, China

Received 10 January 2020/Accepted 24 March 2020/Published online 9 May 2020

Abstract In this paper, we propose a low-complexity frequency slicing deep neural network (FSDNN) for wide-band signal post-equalization in a 1.2 m underwater visible light communication system. FSDNN and deep neural network (DNN) outperform the least mean square equalizer. Then, by splitting the received signal into two parallel signals using a digital low-pass filter and a high-pass filter, we demonstrate that the FSDNN significantly reduces the complexity of the traditional DNN post-equalizer. Moreover, the complexity of the FSDNN decreases considerably to 11.15% compared with the conventional DNN for a 2.7 Gbit/s wide-band transmitted signal with a similar bit error ratio performance.

Keywords deep neural network, frequency slicing, underwater visible light communication, visible light communication

Citation Chi N, Hu F C, Li G Q, et al. AI based on frequency slicing deep neural network for underwater visible light communication. *Sci China Inf Sci*, 2020, 63(6): 160303, <https://doi.org/10.1007/s11432-020-2851-0>

1 Introduction

There is significant increase in the interest of underwater visible light communication (UVLC) systems recently, offering the higher transmission rate and the longer transmission distance compared to the acoustic communication and the radio frequency (RF) transmission [1]. In addition to the benefits of eye-safe, low-latency, and license-free, LED-based UVLC demonstrates high robustness through a giga-bit-per-second capacity of underwater error-free transmission in many studies [2–6]. Among these studies, the advanced modulation formats, such as discrete multi-tone (DMT) and pulse amplitude modulation (PAM), significantly improved the transmission performance of the UVLC system. An alternative to DMT and PAM is a carrierless amplitude and phase (CAP) modulation. This scheme was proposed in VLC, showing a relatively lower complexity and peak-to-average ratio as compared to orthogonal frequency division multiplexing (OFDM) in [7]. Moreover, the CAP modulation with quadrature-amplitude-modulation (QAM) theoretically has higher spectral efficiency compared to PAM with only the amplitude information of signal [8]. Except for the advanced modulation format, various equalization schemes, especially the artificial intelligence (AI) based deep neural network (DNN), can significantly increase the spectral efficiency of the optical communication systems [9,10]. From the superior ability to fit complicate nonlinear functions, the DNN becomes a promising equalizer at the receiver side of the VLC systems. Zhao et al. [6] utilized Gaussian kernel-aided DNN (GKDNN) as a post-equalizer to achieve 1.5 Gbit/s high-speed PAM-8 UVLC. Furthermore, Li et al. [11] achieved 2.4 Gbit/s CAP-modulated VLC system with the DNN post-equalizer over 1.1 m free-space link. Though the DNN confirms a better equalization performance than other traditional adaptive equalizers in many optical communication scenarios [5,12], the

* Corresponding author (email: nanchi@fudan.edu.cn)

high computation complexity of the proposed DNN constrains its wide-spread application. Hence, designing a low-complexity DNN with outstanding equalization performance requires further investigations using LED-based UVLC systems.

Therefore, in this paper, we design and propose a low-complexity frequency slicing DNN (FSDNN), as the first-stage post-equalizer in our 1.2 m CAP-UVLC system. Inside the FSDNN, two finite impulse response filters are utilized to split the received wide-band signal into two parallel narrow-band signals, which are expected to relieve the equalization pressure for followed DNN. Thus, the complexity of the FSDNN is decreased to a lower value than the traditional method using a single DNN to equalize the whole-band signal. For proof of concept, a 2.7 Gbit/s wide-band CAP-QAM-64 signal with the bias current of 135 mA and the peak-to-peak voltage of 0.9 V is transmitted over 1.2 m UVLC link. The performance of the least mean square (LMS) equalizer, Volterra nonlinear equalizer, tradition DNN and FSDNN are fairly compared in the same condition. The experimental results demonstrate not only that both the FSDNN and DNN outperform LMS and Volterra equalizer, but also the complexity of the FSDNN significantly decreases to the 11.15% compared with the traditional DNN. Aslo, a simple structure of the FSDNN adds more robustness when varying peak-to-peak voltage (V_{pp}) and bias current.

2 Principle

The underwater channel brings a big challenge for high-speed transmission due to its higher attenuation as compared to the common free-space channel. Specifically, the power attenuation for blue light in water is 0.4 (ocean)–11 (turbid) dB/m [13]. Conversely, the attenuation for clear air with visibility of 20 km is only 0.0007 dB/m at the wavelength of 650 nm [14], which is much lower than the underwater channel. More details of the underwater channel information can be studied in [13, 15, 16]. Based on the characteristics of the underwater channel and optoelectronic devices, there exists several linear and nonlinear distortion in the UVLC system. First, LED is a bandwidth-constraints optoelectronic component with only around 20 MHz bandwidth if pre-equalization technology is not applied [17]. This nature of LED brings severe frequency fading issue observed in Figure 1(a). There is an apparent amplitude attenuation at the high-frequency domain of the received signal (Rx), resulting in the unignored inter-symbol-interference (ISI) among time-domain symbols. Further more, the nonlinearity of the UVLC also constrains the high-speed transmission, which is mainly induced using the nonlinear electro-optic response of the LED [5], the nonlinear amplification of electrical amplifier [18], and the square-law detection of photodiode [19]. Damaged by these nonlinear effects, the constellation of the received signal at the V_{pp} of 0.9 V (Figure 1(b)) is no longer as the standard lattice structure as that at the V_{pp} of 0.7 V (Figure 1(b)), causing extra symbol errors during the hard decision step. To comprehensively equalize the linear and nonlinear distortion, the DNN serves as an outstanding nonlinear post-equalizer due to its unique multi-layer structure, back-propagation algorithm and the advanced activation function. However, the neural network (NN) must be complex enough to handle the complicated linear and nonlinear distortions, which are explicitly hidden in a wide-band signal. For example, the DNN in Figure 2 of Ref. [4] is with three hidden layers and more than 100 nodes in every hidden layer to guarantee its adaptive equalization ability.

In fact, the damage to the high-frequency and low-frequency domain of the received signal is different, suggesting that the complexity of the DNN can be relieved if these two parts of signals are equalized separately. It is obviously observed that the frequency response of the received signal between 50 MHz and 300 MHz is relatively even as compared to the high frequency range (300–500 MHz) in Figure 1(a). If we consider two uniform root-raise-cosine (RRC) filters $f_1(t)$ and $f_2(t)$ (filters 1 and 2 in Figure 2) with the roll off factor of 0.1 and the length of 165. Their central frequency point is respectively $(\frac{(1+rf)\times BW}{4} + \frac{Z}{2})$ and $(\frac{3\times(1+rf)\times BW}{4} + \frac{Z}{2})$. The BW, rf and Z represent the bandwidth of the transmitted signal, roll-off factor of the CAP signal (0.205), and a few abandoned low-frequency bandwidth (30 MHz), respectively. The subband signals $S_1(t)$ and $S_2(t)$ are obtained by filtering the received signal $R(t)$ with filters 1 and 2. Their relation can be expressed as

$$S_i(t) = R(t) \otimes f_i(t), \quad i = 1, 2, \quad (1)$$

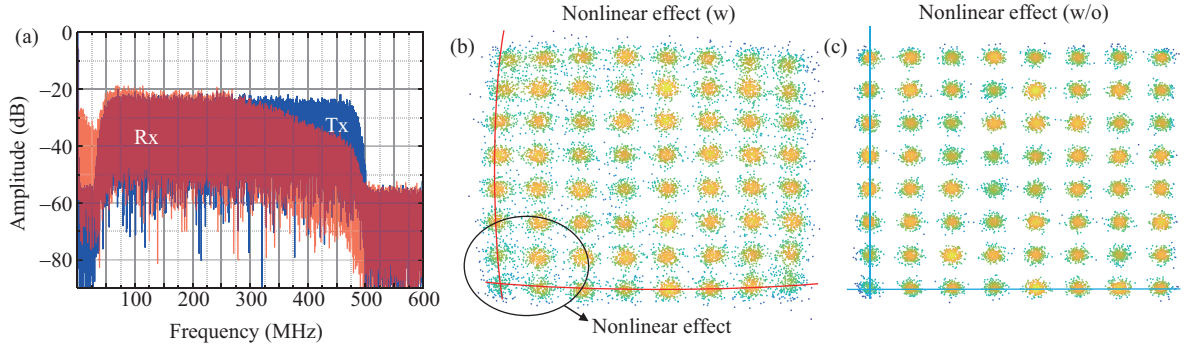


Figure 1 (Color online) (a) The frequency response of received CAP signal (Rx) and transmitted CAP signal (Tx) with the bandwidth of 450 MHz in our UVLC system. The constellation comparison in the case (b) with nonlinear effect and (c) without nonlinear effect in the UVLC system (w: with. w/o: without).

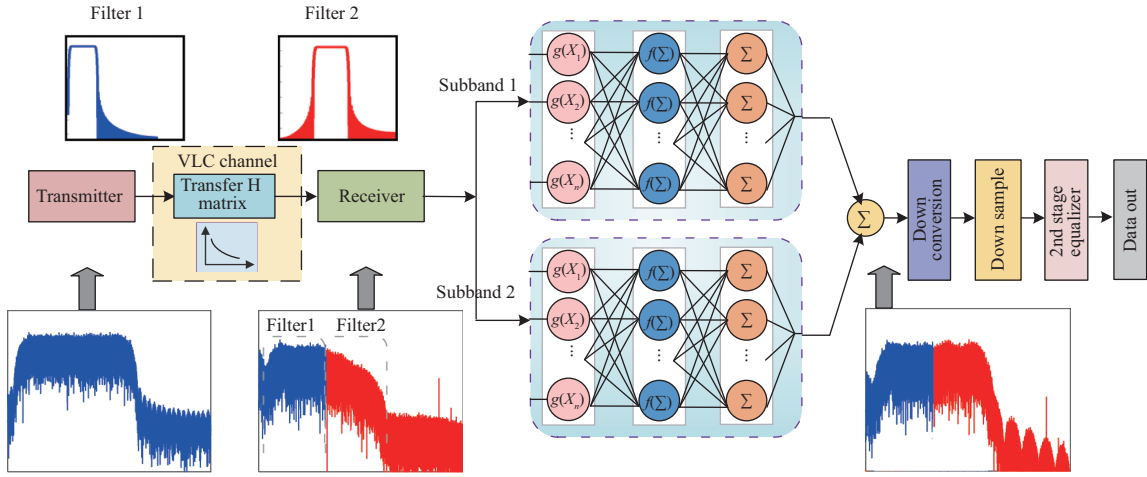


Figure 2 (Color online) The schematic of FSDNN.

where \otimes represents the convolution operation. The two subband signals are then equalized by their own fully-connected DNNs. After reassembling two output signals from DNN through a simple addition process, the equalized signal after FSDNN satisfies that

$$E(t) = D_1(S_1(t)) + D_2(S_2(t)), \quad (2)$$

where $D_i(\cdot)$ denotes the equalization operation of the i -th DNN. At the addition step, the selection of the cut off frequency for $f_1(t)$ and $f_2(t)$ significantly influences the quality of the recovered signal. Cut off frequency mainly depends on the bandwidth and roll-off parameter of the filter. Therefore, the bandwidth BW_1 of both $f_1(t)$ and $f_2(t)$ can be defined as

$$BW_1 = \frac{BW \times \text{sps}_1}{\text{sps}_2}, \quad (3)$$

where sps_1 and sps_2 are respectively defined as the samples per symbols for shaping filter and for $f_1(t)$ and $f_2(t)$. The sps_1 in this study is 4. If the sps_2 is 8, which means BW_1 is exactly half of the width of the shaping filter. No spectrum overlapping exists between $f_1(t)$ and $f_2(t)$. Hence, a drop occurs in the middle of the spectrum for $E(t)$ after the addition process. Similarly, if sps_2 is 6, too much spectrum overlapping will cause a small peak in the middle of the spectrum for $E(t)$. All these cases result in signal distortion. According to the results in Figure 3, the suitable value of sps_2 is 7. Next, the roll-off factor can be slightly tuned to obtain an optimal shape of the spectrum. From Figure 2, most of the high-frequency fading from the channel is well compensated after the FSDNN. The normal CAP demodulation is followed after such first-equalization of FSDNN. For the conventional DNN equalization scheme, it has been specifically states in [4, 6, 11].

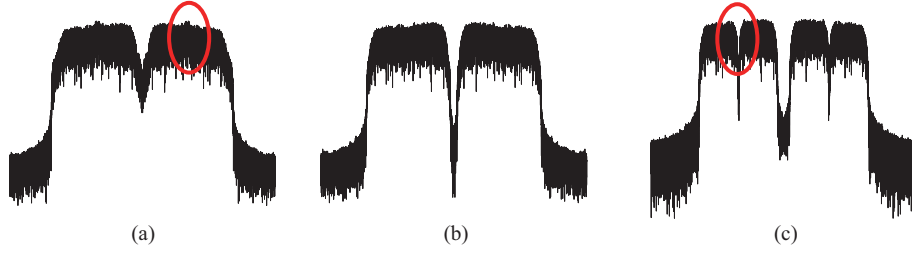


Figure 3 (Color online) The frequency spectrum of recovered signal when (a) sps = 6, (b) sps = 7, (c) sps = 8.

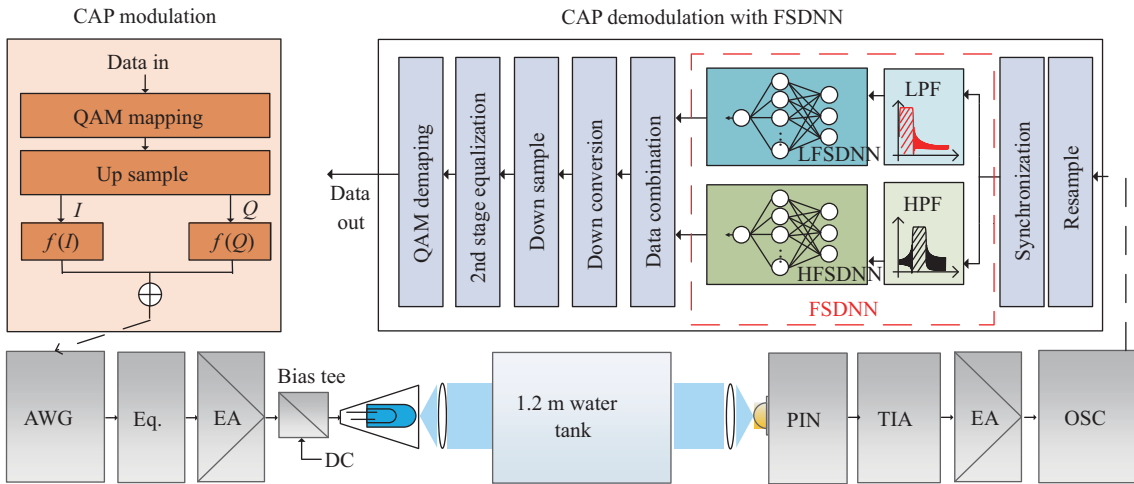


Figure 4 (Color online) Experimental setup. AWG: arbitrary wave generator. EA: electrical amplifier. Eq.: Equalizer. TIA: trans-impedance amplifier. OSC: oscilloscope. LPF: low pass filter. HPF: high pass filter. LFSDNN: the sub-FSDNN with the low-pass filter. HFSDNN: the sub-DNN with the high-pass filter.

3 Experimental setup

Figure 4 shows the experimental set up of the FSDNN-aided CAP modulation LED-UVLC system. The original bit sequence of a data stream gets mapped into the 64-QAM signal. After 4-times up-sampled, the in-phase (I) part and quadrature (Q) components of the up-sampled sequence are filtered accordingly using digital pulse shaping filters $f(t)$ [20]. The outputs of the filters are subtracted to generate the time-domain CAP-QAM-64 signal sequence. Moreover, the generated signal sequence is fed into the arbitrary wave generator (Tektronix AWG710B) to convert a digital signal with a specific sample rate to the analog electrical signal. Through hardware equalization [17] and amplified using a commercial power amplifier (mini circuits ZHL-6A-S+), the electrical signal is coupled with direct current bias by a bias-tee (mini circuits ZFBT-4R2GW-FT+) to drive a blue LED manufactured by Nanchang University. Two collimation lenses are put in a 1.2 m underwater transmission path. The optical signal is captured using a PIN photodiode (Hamamatsu 10784) and transformed into an electrical signal. The signal is also amplified using the trans-impedance amplifier (TIA) and power amplifier. Finally, the signal is resampled using an oscilloscope (KEYSIGHT DSO9404A) for further digital signal processing (DSP). At the DSP part, the resampled signal sequence is first synchronized and then fed into the FSDNN to do the first-stage equalization. The equalized signal is then down-converted from the real signal to the complex signal using the matched filters $g(t)$ with relations as $g(t) = f(-t)$. After down-conversion and down-sample, the complex signal goes through a LMS adaptive filters serving as a 2nd stage equalizer to deal with the residual linear distortion. Finally, the data sequence is recovered using the QAM de-mapping.

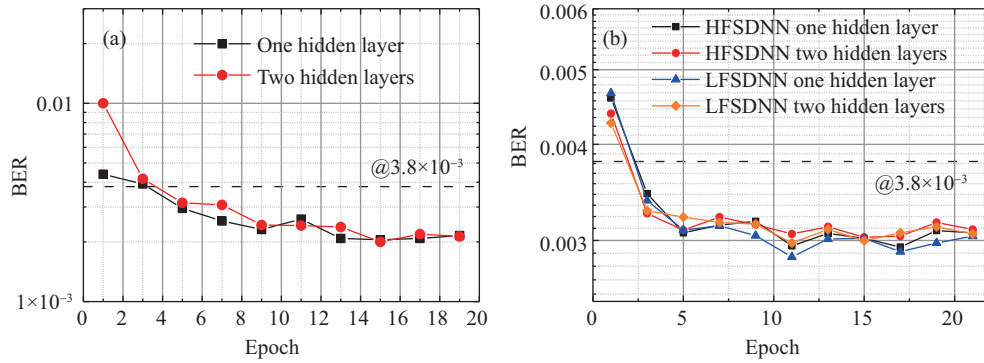


Figure 5 (Color online) BER results versus epoch when (a) DNN has one or two hidden layers, (b) FSDNN has one or two hidden layers.

4 Results and discussion

In order to reach the best transmission performance in CAP-UVLC system, the parameters of the two-stage post-equalizers should be fixed to the optimal values. In this section, we discuss the following three main factors in detailed according to the adjustable parameters of NN [21]:

- (1) The number of layers of the DNN and FSDNN.
- (2) The number of nodes in every layer of the DNN and FSDNN.
- (3) The best taps and step size (u) in the 2nd-stage LMS equalizer.

Once the optimal structure of the FSDNN and DNN is fixed, the comparison of bit error ratio (BER) performance at different V_{pp} and bias current, as well as the convergence speed are followed. Thus, assuming one of the DNN inside the FSDNN equalizing the low-frequency signal is named LFSDDN, the other one equalizing the high-frequency signal gets named HFSDNN. The training of NN depends on the train set. The measurement of the BER performance is based on the test set and the NN after training. Hence, overlapping does not occur on the data set among the train set and test set.

Figure 5 shows the BER performance of the DNN and FSDNN when they have one or two hidden layers. The other parameters, except for the number of layers, are initially kept constant. To prevent the DNN from underfitting due to the simple structure, the number of the input nodes, and nodes in each hidden layer and output layer is 15, 64, and 1, respectively. Therefore, only the number of layers is adjustable. For the FSDNN, a relatively complicate LFSDDN is initially fixed to look for the optimal number of layers in the HFSDNN. Then, the optimal number of HFSDNN is determined in the same method. The results in Figure 4 demonstrate both the DNN and FSDNN with two hidden layers reaching the similar equalization performance with only one hidden layer. However, when epoch increases, the BER performance approaches a fixed value, suggesting no underfitting and overfitting problem happening, and only one hidden layer is enough to cope with the distortion in time-domain in the least complexity penalty.

Next, the optimal taps of the DNN and FSDNN are determined when fixing the number of the hidden layer and epoch is 64 and 15, respectively. As the taps of the DNN get rising, the DNN considers a broader range of interference between the symbols. Accordingly, the BER gets decreasing (Figure 6(a)). However, the degree of symbol distortion induced by the ISI and system nonlinearity is finite, the optimal taps of DNN is 21. The longer taps will not bring more gain in the BER performance. For the FSDNN, the best taps of the HFSDNN and LFSDDN are 5 and 3, respectively, which is smaller than the DNN because the input data sequence is a narrowed signal instead of a wide-band signal. There is less distortion in the narrow-band signal requiring fewer taps in the FSDNN to handle as compared to the DNN.

After fixing the number of layers, taps, the number of nodes in the hidden layer influences the regression ability of the DNN for dealing with the linear and nonlinear damage. Few nodes will weaken the study ability of the NN. However, too many nodes will increase the complexity of the NN, still, distortion is hardly mitigated completely limited by the update algorithm, the scale of the train set and the random

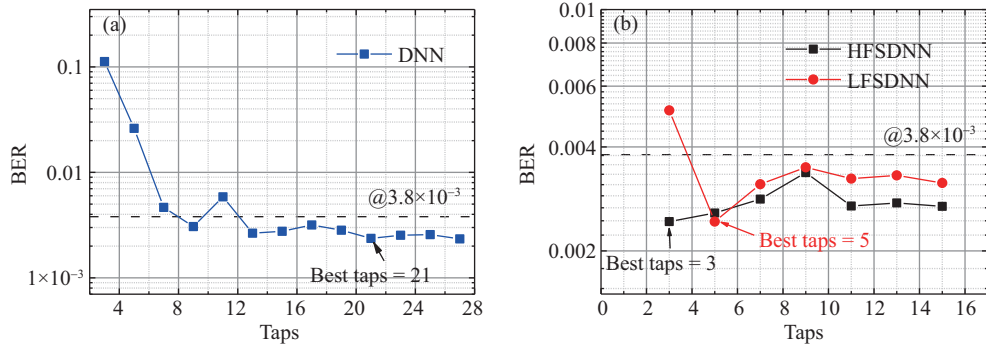


Figure 6 (Color online) BER performance versus different taps of (a) DNN and (b) FSDNN, including HFSDNN and LFSDNN. Taps is the number of input nodes in input layer.

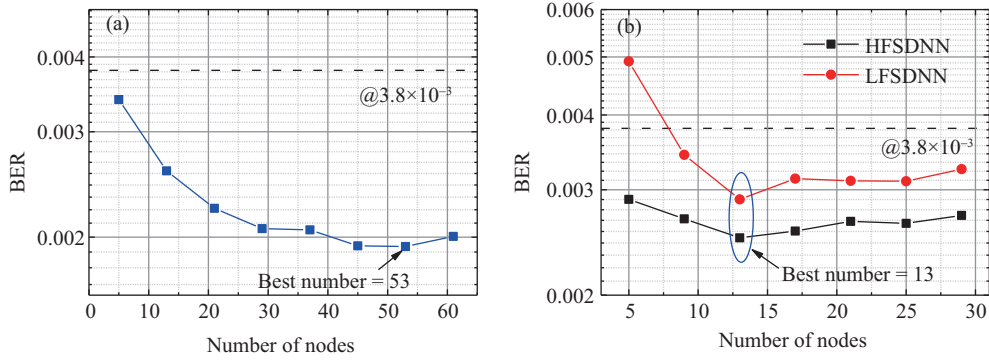


Figure 7 (Color online) BER performance versus different number of nodes in hidden layer of (a) DNN and (b) FSDNN.

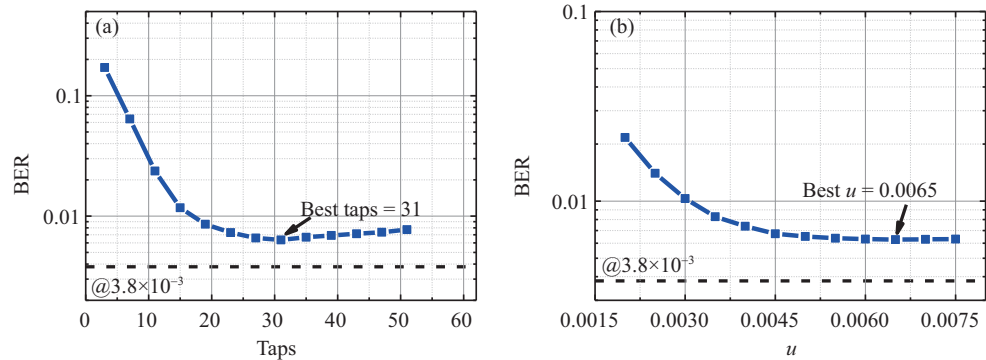


Figure 8 (Color online) BER performance versus different (a) taps and (b) step size (u) in the 2nd-stage LMS equalizer.

Gaussian white noise, indicating the BER will fluctuate around a fixed value when the number of nodes increases. Therefore, the best number of nodes in the DNN, HFSDNN and LFSDNN is 53, 13 and 13, respectively (Figure 7).

From the earlier discussion, the optimal structure of the DNN and FSDNN is both 3-layer structure, respectively with nodes of 21, 53, 1 and 5, 13, 1 for HFSDNN and 3, 13, 1 for LFSDNN in every layer. Based on the structure without the first-stage equalizer, we also iterate the taps and step length (u) of LMS equalizer to find the best structure of LMS equalizer (Figure 8). Similarly, the best taps and u are 31 and 0.0065 since the LMS equalizer is only a linear equalizer with limited equalization performance.

The optimal structure of the DNN and FSDNN is established at the V_{pp} of 0.9 V and the current of 135 mA. In order to prove the robustness and efficiency of the FSDNN at other V_{pp} and current, we compare the BER performance of LMS, Volterra, DNN plus the LMS and FSDNN plus LMS at other V_{pp} and currents with the same network structure. The results are plotted in Figure 9, showing that

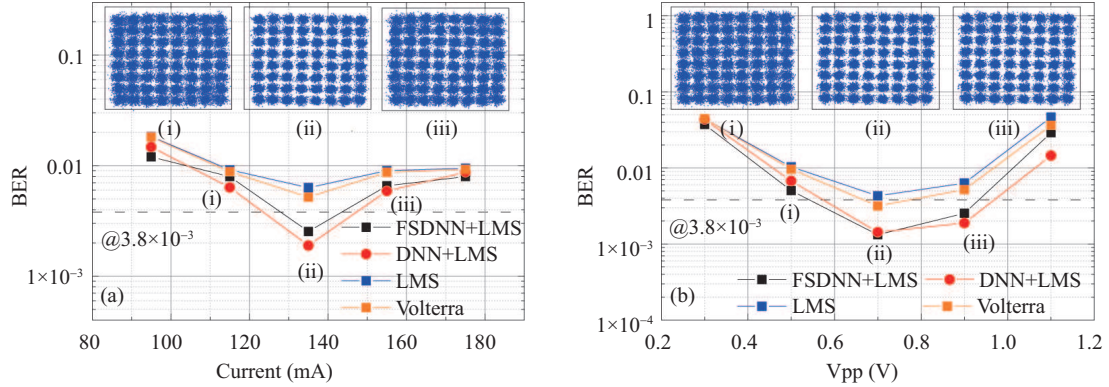


Figure 9 (Color online) BER performance versus (a) different bias current and (b) V_{pp} for LMS, Volterra, DNN plus LMS and FSDNN plus LMS under the optimal structure. Insets: the constellation of the equalized signal using FSDNN at the certain V_{pp} of (i) 0.5 V, (ii) 0.7 V, (iii) 0.9 V and at the certain current of (i) 115 mA, (ii) 135 mA, (iii) 155 mA.

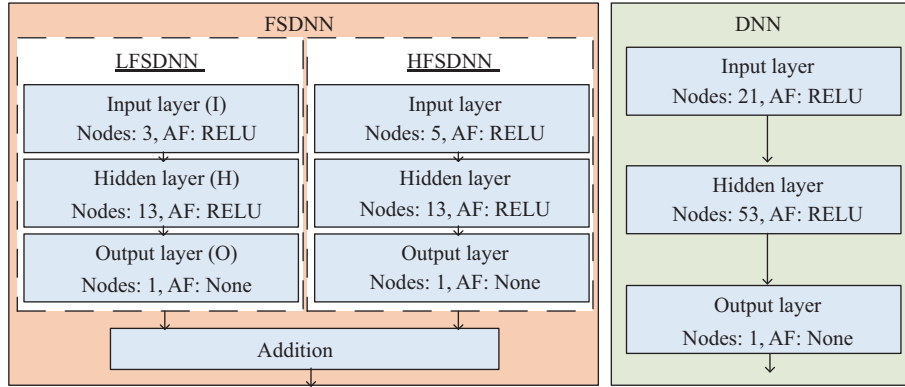


Figure 10 (Color online) The structure of optimal DNN and FSDNN. I: input layer. H: hidden layer. O: output layer.

the FSDNN has similar BER performance as the DNN, and both of them successfully lower the BER of the case only with LMS post-equalizer. When the V_{pp} is around 0.3 V, the UVLC system is mainly restrained by the low signal-to-noise ratio (SNR). The enhancement from DNN and FSDNN is little because the random Gaussian white noise cannot be well fitted and combated using the NN. Adversely, DNN and FSDNN significantly reduce the BER when the V_{pp} is at 0.5 V and 0.7 V, since the linear distortion like the ISI becomes the main limitation to the UVLC as the SNR increasing. When V_{pp} is higher than 0.9 V, the high amplitude of signal brings the severe nonlinear effect which consists of the high order of signals, such as the square and the cubic of signal amplitude [22]. Though the complexity of the FSDNN is lower than the DNN, the DNN has better nonlinear resistance than FSDNN because it has the information of the whole wide-band signal to facilitate fitting the nonlinearity. Then, each FSDNN is only trained by part of the wide-band signal. When the current changes from 95 mA to 175 mA, the BER of FSDNN is at a similar level with DNN in general. However, at the current of 95 mA and 175 mA, which are the currents farthest than 135 mA, the FSDNN outperforms DNN due to its simple structure, which brought better robustness.

Finally, we conclude the optimal structure and complexity analysis of the DNN and FSDNN in Figure 10. In this paper, we use spatial complexity which is the number of weight parameters needed to update during the update process to stand for the complexity of them. Derived from [23], the complexity of the NN is $I \times H + H \times O$. Therefore, the complexity of FSDNN is $(3 \times 13 + 13 \times 1) + (5 \times 13 + 13 \times 1) = 130$. Further, the complexity of the DNN is $(21 \times 53 + 53 \times 1) = 1166$, which is almost 9 times compared with the FSDNN. Using the method of the frequency slicing, the complexity of the FSDNN shrinks to 11.15% of that of the DNN.

5 Conclusion

We first designed and proposed a low-complexity FSDNN which has a better equalization performance compared to the LMS equalizer and similar equalization performance as the traditional DNN. Moreover, by introducing two root raised cosine (RRC) filters to split the wide-band signal into two narrow-band signals, the method of frequency slicing successfully suppresses the pressure during the NN training. Further more, we discussed the optimal structure of the DNN and FSDNN at the Vpp of 0.9 V and the current of 135 mA. Based on the optimal structure, we confirmed the complexity of the FSDNN only to be 11.15% compared with the DNN. Aslo, the FSDNN has a similar equalization performance with the DNN at other Vpps and currents. Although the DNN has better nonlinear resistance, the FSDNN shows superior robustness than DNN, whereas linear noise is the main limitation of the UVLC system.

Acknowledgements This work was partially supported by National Key Research and Development Program of China (Grant No. 2017YFB0403603) and Natural National Science Foundation of China (Grant No. 61925104).

References

- 1 Zeng Z Q, Fu S, Zhang H H, et al. A survey of underwater optical wireless communications. *IEEE Commun Surv Tut*, 2017, 19: 204–238
- 2 Chi N, Haas H, Kavehrad M, et al. Visible light communications: demand factors, benefits and opportunities. *IEEE Wirel Commun*, 2015, 22: 5–7
- 3 Zhou Y J, Zhu X, Hu F C, et al. Common-anode LED on a Si substrate for beyond 15 Gbit/s underwater visible light communication. *Photon Res*, 2019, 7: 1019–1029
- 4 Zhao Y H, Zou P, Yu W X, et al. Two tributaries heterogeneous neural network based channel emulator for underwater visible light communication systems. *Opt Exp*, 2019, 27: 22532–22541
- 5 Chi N, Hu F C. Nonlinear adaptive filters for high-speed LED based underwater visible light communication. *Chin Opt Lett*, 2019, 17: 100011
- 6 Chi N, Zhao Y, Shi M, et al. Gaussian kernel-aided deep neural network equalizer utilized in underwater PAM8 visible light communication system. *Opt Exp*, 2018, 26: 26700–26712
- 7 Wu F M, Lin C T, Wei C C, et al. Performance comparison of OFDM signal and CAP signal over high capacity RGB-LED-based WDM visible light communication. *IEEE Photon J*, 2013, 5: 7901507–7901507
- 8 Ziemer R E, Tranter W H. *Principles of Communications*. Hoboken: John Wiley Sons, 2014
- 9 Zibar D, Piels M, Jones R, et al. Machine learning techniques in optical communication. *J Lightw Technol*, 2016, 34: 1442–1452
- 10 Khan F N, Lu C, Lau A P T. Machine learning methods for optical communication systems. In: *Proceedings of Signal Processing in Photonic Communications*, 2017. 3
- 11 Li G, Hu F, Zhao Y, et al. Enhanced performance of a phosphorescent white LED CAP 64QAM VLC system utilizing deep neural network (DNN) post equalization. In: *Proceedings of IEEE/CIC International Conference on Communications in China (ICCC)*, Changchun, 2019. 173–176
- 12 Osahon I N, Rajbhandari S, Popoola W O. Performance comparison of equalization techniques for SI-POF multi-Gigabit communication with PAM-M and device non-linearities. *J Lightw Technol*, 2018, 36: 2301–2308
- 13 Kaushal H, Kaddoum G. Underwater optical wireless communication. *IEEE Access*, 2016, 4: 1518–1547
- 14 Ali M A A, Mohammed M A. Effect of atmospheric attenuation on laser communications for visible and infrared wavelengths. *Al-Nahrain J Sci*, 2013, 16: 133–140
- 15 Johnson L, Green R, Leeson M. A survey of channel models for underwater optical wireless communication. In: *Proceedings of 2013 2nd International Workshop on Optical Wireless Communications (IWOW)*, 2013. 1–5
- 16 Cossu G. Recent achievements on underwater optical wireless communication. *Chin Opt Lett*, 2019, 17: 100009
- 17 Huang X X, Wang Z X, Shi J Y, et al. 1.6 Gbit/s phosphorescent white LED based VLC transmission using a cascaded pre-equalization circuit and a differential outputs PIN receiver. *Opt Express*, 2015, 23: 22034–22042
- 18 Kim J, Konstantinou K. Digital predistortion of wideband signals based on power amplifier model with memory. *Electron Lett*, 2001, 37: 1417–1418
- 19 Ju C, Liu N, Chen X, et al. SSBI mitigation in A-RF-tone-based VSSB-OFDM system with a frequency-domain volterra series equalizer. *J Lightw Technol*, 2015, 33: 4997–5006
- 20 Zhang J W, Yu J J, Li F, et al. 11×5×9.3 Gb/s WDM-CAP-PON based on optical single-side band multi-level multi-band carrier-less amplitude and phase modulation with direct detection. *Opt Exp*, 2013, 21: 18842–18848
- 21 Burse K, Yadav R N, Shrivastava S C. Channel equalization using neural networks: a review. *IEEE Trans Syst Man Cybern C*, 2010, 40: 352–357
- 22 Zhou Y, Zhang J, Wang C, et al. A novel memoryless power series based adaptive nonlinear pre-distortion scheme in high speed visible light communication. In: *Proceedings of Optical Fiber Communication Conference and Exhibition (OFC)*, 2017
- 23 Haykin S O. *Neural Networks and Learning Machines*. Upper Saddle River: Pearson, 2009. 3